ADVANCES IN ATMOSPHERIC SCIENCES, VOL. 26, NO. 2, 2009, 333–342

The ENSO's Effect on Eastern China Rainfall in the Following Early Summer

LIN Zhongda* (林中达) and LU Riyu (陆日宇)

Center for Monsoon System Research, Institute of Atmospheric Physics,

Chinese Academy of Sciences, Beijing 100029

(Received 25 January 2008; revised 22 May 2008)

ABSTRACT

ENSO's effect on the rainfall in eastern China in the following early summer is investigated by using station precipitation data and the ERA-40 reanalysis data from 1958 to 2002. In June, after the El Niño peak, the precipitation is significantly enhanced in the Yangtze River valley while suppressed in the Huaihe River-Yellow River valleys. This relationship between ENSO and the rainfall in eastern China is established possibly through two teleconnections: One is related to the western North Pacific (WNP) anticyclonic anomaly in the lower troposphere leading to enhanced precipitation in the Yangtze River valley, and the other is related to the southward displacement of the Asian jet stream (AJS) in the upper troposphere resulting in suppressed precipitation in the Huaihe River-Yellow River valleys.

This southward displacement of the AJS is one part of ENSO's effect on the zonal flow in the whole Northern Hemisphere. After the El Niño peak, the ENSO-related warming in the tropical troposphere persists into the following early summer, increasing the meridional temperature gradient and through the thermal wind balance, leads to the enhancement of westerly flow in the subtropics south of the westerly jet stream and results in a southward displacement of the westerly jet stream.

Key words: ENSO, eastern China rainfall, early summer, Asian jet stream, western North Pacific anticyclone

Citation: Lin, Z. D., and R. Y. Lu, 2009: The ENSO's effect on eastern China rainfall in the following early summer. *Adv. Atmos. Sci.*, **26**(2), 333–342, doi: 10.1007/s00376-009-0333-4.

1. Introduction

The El Niño-Southern Oscillation (ENSO) has the greatest impact on the year-to-year variability of the global climate (Webster et al., 1998). The mature phase of ENSO often peaks in boreal winter, persists into spring, and decays in the following summer. The East Asian monsoon system, as one of the most active components of global climate system, is significantly affected by ENSO (Tanaka, 1997; Zhang et al., 1999; Wang et al., 2000; Lau et al., 2000; Wang et al., 2001; Ha and Ha, 2006).

The effect on summer rainfall in East Asian depends on the phase of the ENSO cycle (Huang and Wu, 1989; Tanaka, 1997; Wu et al., 2003). Wu et al. (2003) indicated that the ENSO-related rainfall anomalies consist of two main centers in eastern China: The decreased rainfall in northern China during the summer and fall in the developing year of El Niño, and the increased rainfall in southern China and east central China from the fall of the developing year of El Niño through the next spring. In the summer after the El Niño peak, the rainfall tends to enhance along the subtropical frontal belt (Chen et al., 1992; Chang et al., 2000; Lau and Weng, 2001).

A majority of the previously mentioned studies of ENSO's effects on the East Asian summer rainfall are based on the June–July–August (JJA) mean. However, the study of ENSO's effects may not be appropriate on the East Asian summer rainfall, especially in eastern China by using the JJA mean data. This is due to the fact that the rain-band in eastern China shows a large meridional excursion in boreal summer: The summer rainy belt in eastern China is located over southern China and the Yangtze River valley in June, and then penetrates into northern China

*Corresponding author: LIN Zhongda, zdlin@mail.iap.ac.cn

in July–August. Given this remarkable sub-seasonal meridional shift, it is reasonable to hypothesize that the ENSO-related summer rainfall in East Asia also exhibits sub-seasonally dependent features, that is, ENSO's effects on the East Asian rainfall in June may be distinct from that in July and August. Actually, Lim and Kim (2007) investigated the ENSO impact on the space-time evolution of the regional Asian summer monsoon by the cyclostationary EOF method. They found an ENSO mode, which is the third largest component (next to the seasonal cycle and intraseasonal oscillation with a 40–50-day period) of the Asian summer monsoon variation, exerts a distinct role in the eastern China rainfall in early summer (late May–June) from that in July. This mode is correlated with the developing stage of the ENSO cycle, indicated by the significant correlation between the corresponding principle component time series and the Niño-3 time series, with the former leading the latter by 5 months. However, the effect of ENSO on the sub-seasonal variation of the eastern China summer rainfall in the decaying phase is not clear.

The variation of ENSO-related eastern China rainfall in the decaying phase is presented in Fig. 1. The ENSO-related precipitation, after an El Niño peak, increases remarkably over the southeast coast of China from January to March, and over a wider area from southern China to northern China in April and May. The ENSO-related precipitation reaches its maximum in June, and it is significantly enhanced in the Yangtze River valley and suppressed in the Huaihe River-Yellow River valleys. In July and August, the precipitation in eastern China is not significantly related to the preceding ENSO, except over northern China where precipitation is slightly enhanced. Therefore, it is reasonable to divide the summer into two periods: early summer (June) and mid summer (July–August), in order to investigate the ENSO-eastern China summer rainfall relationship. In this study, we focus on the effects that ENSO has on the rainfall anomalies in early summer, which are more significant and stronger.

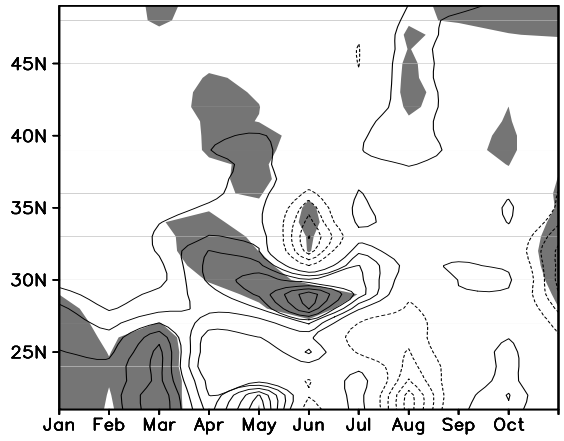

Fig. 1. Monthly precipitation averaged in eastern China (110°–120°E) regressed onto the preceding wintertime (December–January–February, DJF) Niño-3.4 index. Shading denotes the significance at the level of 0.05, contour interval is 5 mm per month, and the zero contours are omitted.

The aim of this study is to investigate the relationship between ENSO and the eastern China rainfall in the following early summer and to discuss the possible mechanisms linking them. In section 2, the description of the data and indexes used in this study are presented. In section 3, we document the characteristics of the ENSO-related precipitation in eastern China and circulation in early summer, and their association with the Pacific-East Asian teleconnection (Wang et al., 2000) through the lower-level WNP anticyclonic anomaly. We find that the WNP anticyclonic anomaly is capable of interpreting the ENSO-related precipitation enhanced in the Yangtze River valley, but not the suppressed precipitation in the Huaihe River-Yellow River valleys. Thus, in section 4 we propose another possible way that ENSO affects the eastern China summer rainfall, through the meridional displacement of the Asian jet stream (AJS) in the upper troposphere. In section 5, we discuss the mechanism linking ENSO and the meridional displacement of the AJS. Finally, the conclusions are given in section 6.

2. Data and indexes

The accumulated monthly 160 station rainfall data from mainland China, provided by the Chinese Meteorological Data Center, is used. In this study, we restrict our analysis of rainfall to the region east of 100°E and south of 45°N, which includes 127 stations (Fig. 2), from the period of 1958–2002.

The monthly atmospheric data comes from the European Center for Medium-Range Weather Forecast (ECMWF) ERA-40 reanalysis data (Uppala et al., 2005). The variables used in this study include zonal and meridional winds, temperature, and geopotential height. This data has a horizontal resolution of $2.5° \times 2.5°$ and the period spans from September 1957 to August 2002.

To study ENSO's effect on the rainfall in eastern China in early summer, the preceding boreal winter (December–January–February, DJF) SST anomalies, averaged over the Niño-3.4 region (5°S–5°N, 170°–120°W), are taken as an index. The Niño-3.4 index data comes from the Climate Prediction Center (CPC). The effect of ENSO on the rainfall in eastern China in early summer is depicted by the lag correla-

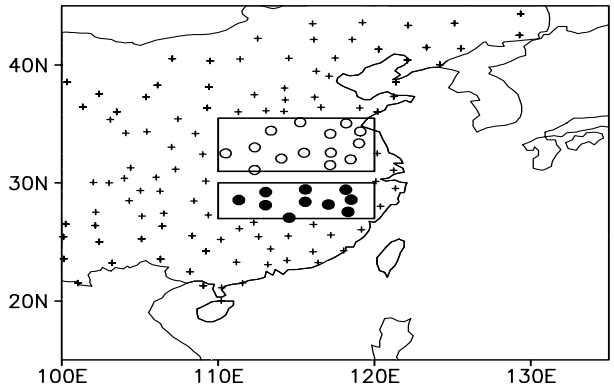

Fig. 2. The locations of 127 Chinese stations used in this study east of 100°E and south of 45°N. The north rectangle represents the Huaihe River-Yellow River valleys (31°–36°N, 110°–120°E) including 14 stations (empty circles) and the south denotes the Yangtze River valley (27°–30°N, 110°–120°E) with 10 stations (filled circles).

tion and regression between the DJF Niño-3.4 index and the following June precipitation. To exclude the effects of interdecadal change, the variability with periods exceeding 8 years has been removed through harmonics analysis before calculating the correlation and regression for the period of 1958–2002.

Two precipitation indexes, referred to as the Yangtze River valley precipitation index (YRPI) and the Huaihe River-Yellow River valleys precipitation index (HYPI), are defined as the precipitation averaged over 27°–30°N, 110°–120°E (including 10 stations) and 31°–36°N, 110°–120°E (including 14 stations) (Fig. 2), respectively, to depict the ENSO-related precipitation anomalies in the following early summer. The western North Pacific summer monsoon index (WNPSMI), which is defined as the difference of averaged zonal winds at 850 hPa between 20°–30°N, 110°–140°E and 5°–15°N, 100°–130°E, is also adopted. The index is the same as the WNPSMI presented by Wang et al. (2001), but with opposite signs. The WNPSMI in this study is positively correlated with the preceding DJF Niño-3.4 index, and thus this minor modulation can facilitate the comparison between ENSO- and the WNPSMI-related anomalies. The first principle component (Pc1) of the EOF analysis on the zonal winds at 200 hPa over 0°–50°N, 0°–150°E in June, corresponding to the meridional displacement of the AJS in the upper troposphere, is adopted to present the other possible way by which ENSO affects the rainfall of eastern China in the following early summer. Note that all the indexes used in this study, including the YRPI, the HYPI, the WNPSMI, and the Pc1, are only for June, except for the Niño-3.4 index in the preceding DJF.

3. Precipitation and circulation anomalies related to ENSO and the WNP anticyclonic anomaly

It has been shown in Fig. 1 that in June, subsequent to ENSO peaks, there is a dipole-like pattern of rainfall anomalies in eastern China. This can be seen more clearly from the horizontal distribution of ENSO-related precipitation in eastern China (Fig. 3). After the El Niño peak, the precipitation remarkably increases in the Yangtze River valley, while decreases in the Huaihe River-Yellow River valleys. Based on this figure, we define the precipitation in June, averaged over 27°–30°N, 110°–120°E and 31°–36°N, 110°–120°E, as the Yangtze River valley precipitation index (YRPI) and the Huaihe River-Yellow River valleys precipitation index (HYPI), with which the correlation coefficients of the DJF Niño-3.4 index are 0.51 and −0.39 (Table 1), respectively, both significant at the

Table 1. Correlation coefficients between the Niño-3.4 SST index, the WNPSMI, the Pc1, the HYPI, and the YRPI during the period 1958–2002. Note that all the indexes, including the YRPI, the HYPI, the WNPSMI, and the Pc1 are only for June, except for the Niño-3.4 index in the preceding DJF. See section 2 of the text for the detailed definitions of the five indexes.

	WNPSMI	Pc1	HYPI	YRPI
Niño-3.4	0.46**	0.37*	−0.39**	0.51**
WNPSMI		0.12	0.13	0.53**
Pc1			−0.42**	0.12
HYPI				−0.17

*(**): significance at the level of 0.05 (0.01).

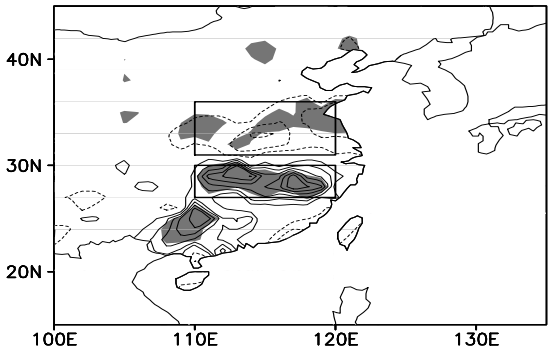

Fig. 3. June precipitation in eastern China regressed onto the preceding DJF Niño-3.4 index. The regions surrounded by the two thick rectangles are the same as Fig. 2. Shading denotes the significance at the level of 0.05, the contour interval is 10 mm per month, and the zero contours are omitted.

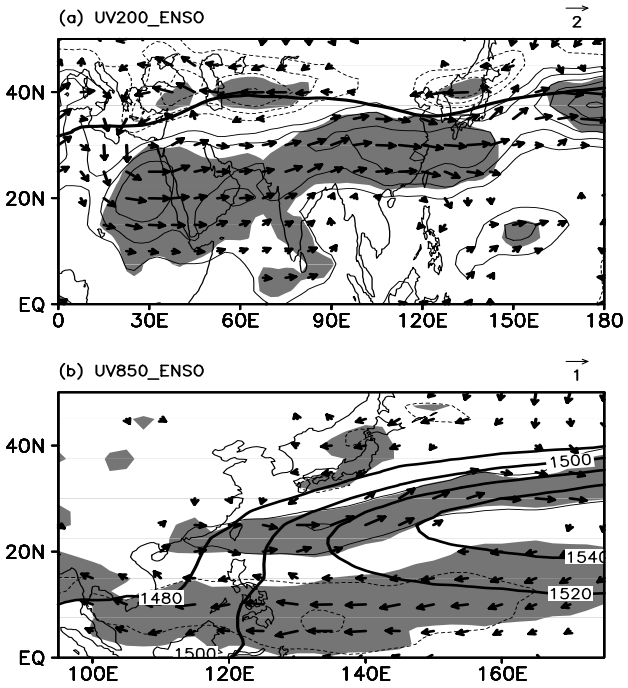

Fig. 4. June horizontal winds (vector) and zonal winds (contour) (a) at 200 hPa and (b) 850 hPa regressed onto the preceding DJF Niño-3.4 index. Shading denotes the significant correlation with the zonal winds at the confidence level of 95% and contour intervals are 0.5 m s^{-1}. The thick black line denotes the axis of the climatological June Asian jet stream (AJS) at 200 hPa in (a) and the climatological June geopotential heights at 850 hPa in (b).

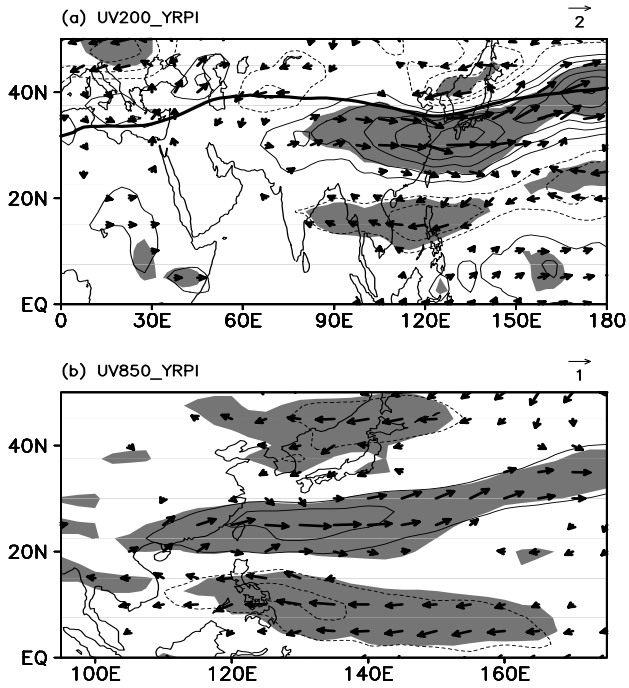

Fig. 5. June horizontal winds (vector) and zonal winds (contour) at (a) 200 hPa and (b) 850 hPa regressed onto the index of June precipitation averaged in the Yangtze River valley (27°E–30°N, 110°–120°E) (YRPI). Shading denotes the significant correlation with the zonal winds at the confidence level of 95%, contour intervals are 0.5 m s^{-1}, and the thick black line in (a) denotes the axis of the climatological June Asian jet stream (AJS) at 200 hPa.

level of 99%. The significant precipitation anomaly is absent in the other regions, except over the southwest coast of China with a smaller-range precipitation increase. Thus, in the next sections we concentrate on the ENSO-related precipitation anomalies in the Huaihe River-Yellow River valleys and the Yangtze River valley.

The ENSO-related precipitation anomalies in eastern China are associated with the southward displacement of the AJS in the upper troposphere and the WNP anticyclonic anomaly in the lower troposphere (Fig. 4). Related to the ENSO peak in the preceding winter, a strong westerly anomaly prevails in the upper troposphere from northeast Africa eastward to East Asia between 10°N and 30°N, corresponding to the strengthening and southward displacement of the AJS (Fig. 4a). In addition, the weak easterly anomalies occur near the axis of the AJS between 35°N and 45°N, which reduce the intensity of the AJS and favor the southward shift. In the lower troposphere, a strong anticyclonic anomaly dominates the WNP from near the dateline westward to about 110°E, which is corresponding to the westward extension of the western North Pacific subtropical high in June (Lu and Dong, 2001). In this study, we adopted the WNPSMI presented by Wang et al. (2001) (see section 2 for the detailed definition) to depict this WNP anticyclonic anomaly. In a year with a positive WNPSMI, an anomalous anticyclone situates itself over the WNP with the westerly anomaly over the subtropical WNP between 20°–30°N, and the easterly anomaly over the WNP between 5°–15°N (see also Fig. 7b). The correlation coefficient between the WNPSMI and the DJF Niño-3.4 index is 0.46, significant at the level of 99% (Table 1). In East Asia, a weak cyclonic anomaly is identified to the south of Japan.

How does ENSO influence the rainfall in June in eastern China as shown in Fig. 3? Wang et al. (2000) proposed a Pacific-East Asian teleconnection, and implied that ENSO influences the East Asian rainfall in early summer through a persistent lower-level anomalous anticyclone over the WNP, which is maintained by the positive local air-sea feedback between the WNP anticyclonic anomaly and *in-situ* SST anomalies

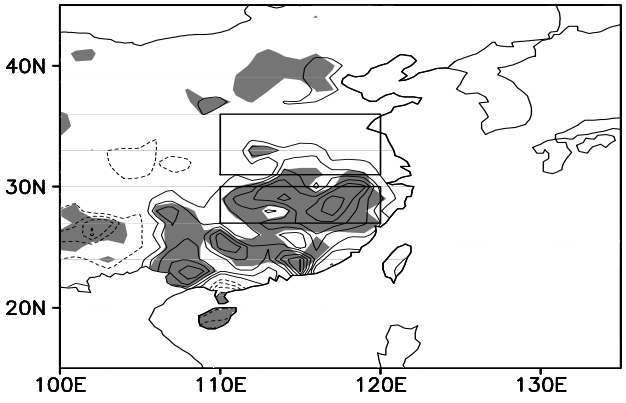

Fig. 6. Same as Fig. 3, but onto the western North Pacific summer monsoon index (WNPSMI) in June, which is defined as the difference of averaged zonal winds at 850 hPa between 20°–30°N, 110°–140°E and 5°–15°N, 100°–130°E , opposite to that defined by Wang et al. (2001).

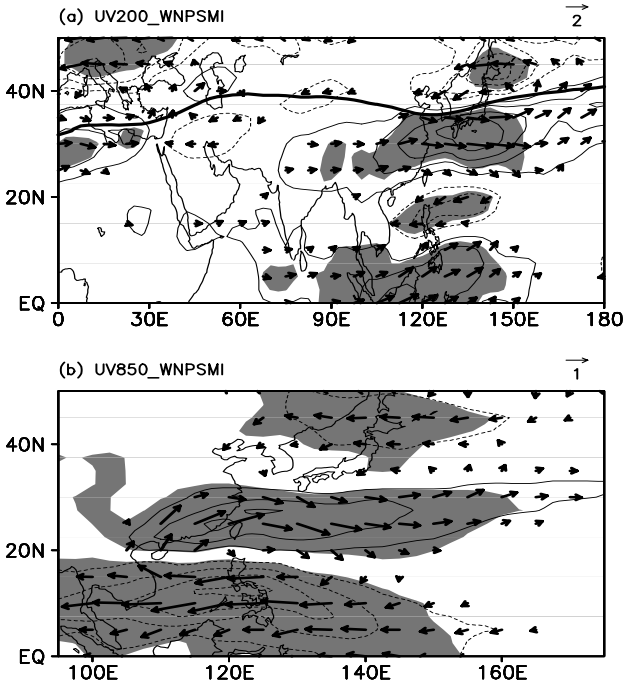

Fig. 7. Same as Fig. 5, but onto the June WNPSMI.

(Wang et al., 2000; Lau et al., 2004). In the summer after the El Niño peak, the rainfall tends to enhance along the subtropical frontal belt (Chen et al., 1992; Chang et al., 2000; Lau and Weng, 2001). Figure 5 shows the horizontal wind anomalies related to the YRPI. The enhanced precipitation in the Yangtze River valley is significantly related to an anticyclonic anomaly over the WNP in the lower troposphere (Fig. 5b). In the upper troposphere, a strong anticyclonic anomaly covers the subtropical WNP and southern China (Fig. 5a), which is possibly due to the direct thermal response to the enhanced precipitation in the Yangtze-River valley.

Moreover, we calculated the WNPSMI-related June precipitation anomalies in eastern China (Fig. 6). Corresponding to an anticyclonic anomaly over the WNP, the precipitation is significantly enhanced in the Yangtze River valley and the correlation coefficient of the WNPSMI with the YRPI is 0.53 (Table 1). The area of enhanced precipitation is much larger than that shown in Fig. 3. For the Huaihe River-Yellow River valleys, however, the precipitation does not exhibit any significant variation related to the WNP anticyclonic anomaly and the correlation coefficient between the WNPSMI and the HYPI is only 0.13 (Table 1). In addition, the precipitation also increases over northern China and decreases over southwestern China.

The WNPSMI is associated with a meridional teleconnection pattern over East Asia-WNP (Fig. 7). The meridional pattern exhibits a baroclinic vertical structure over the WNP and roughly a barotropic structure in East Asia, resembling a Pacific-Japan (PJ) pattern or an East Asia-Pacific (EAP) pattern (Nitta, 1987; Huang and Sun, 1992; Kosaka and Nakamura, 2006). In the lower troposphere, a strong anticyclonic anomaly dominates the WNP and a weak cyclonic anomaly appears in East Asia. The lower-level southwesterly anomaly over the Yangtze River valley strengthens the climatological southwesterlies, and thus transports more moisture into this region, favoring precipitation enhancement. The southwesterly anomaly is much stronger and occupies a wider area than that associated with ENSO (Fig. 4b), which may be the reason for the fact that the enhanced precipitation associated with the WNPSMI (Fig. 6) is stronger and in a larger area than that associated with ENSO (Fig. 3). In the upper troposphere, the cyclonic anomaly in East Asia, with an anomalous westerly over 25°–35°N and an anomalous easterly over 40°–50°N, is related to the southward displacement of the East Asian westerly jet stream in June (Lu, 2004; Lin and Lu, 2005).

The results in this section indicate that the lower-level WNP anticyclonic anomaly and the associated PJ-like pattern significantly contribute to the ENSO-related increased precipitation in the Yangtze River valley, but not to the decreased precipitation in the Huaihe River-Yellow River valleys. In the upper troposphere the WNPSMI-related zonal wind anomalies consist of a meridional four-cell structure, with the zonal wind anomalies mostly confined to the east of 110°E over East Asia-WNP (Fig. 7a). In contrast, the ENSO-related westerly anomaly exhibits a much larger zonal extension from about 20°E eastward to

150°E (Fig. 4a). In the lower troposphere, the anticyclonic anomaly over the WNP is restricted to the west of 140°E, related to the WNPSMI (Fig. 7b), while it extends to the dateline related to ENSO (Fig. 4b).

4. Effect of meridional displacement of the AJS on the eastern China summer rainfall

Figure 8 shows the horizontal wind anomalies related to the minus HYPI. Corresponding to the suppressed precipitation in the Huaihe River-Yellow River valleys, the AJS shifts southward. The westerly anomaly emanates from northeast Africa eastward to East Asia in the subtropics, while the easterly anomaly moves to the north from east of the Mediterranean Sea to northeast Asia in the mid latitudes, in an analogous fashion related to ENSO (Fig. 4a). The similarity suggests that ENSO may link the suppressed precipitation in the Huaihe River-Yellow River valleys by the southward displacement of the AJS over the mid-latitudes in Asia. In the lower troposphere, an isolated cyclonic anomaly is located over the subtropical WNP.

We performed an EOF analysis on the zonal winds at 200 hPa over 0°–50°N, 0°–150°E in June. The first mode denotes the meridional displacement of the AJS (Fig. 9), closely resembling the zonal wind anomalies in the upper troposphere related to ENSO (Fig. 4a) and the minus HYPI (Fig. 8a). Years with positive and negative values of the first principle component (Pc1) are referred to as the positive and negative phase, respectively. During the positive phase, the westerly anomaly lies to the south of the axis of the AJS and the easterly anomaly to the north, corresponding to the southward displacement of the AJS. During the negative phase, the AJS shifts northward. This meridional displacement of the AJS is also confirmed by the composite zonal winds at 200 hPa averaged over 0°–150°E based on the Pc1 (figure is not shown). In the 7 years with Pc1 larger than 1 standard deviation, the axis of the AJS is located at 35°N, while at about 37.5°N in the 9 years with Pc1 less than −1 standard deviation.

The meridional displacement of the AJS is significantly correlated to ENSO with a correlation coefficient of 0.37 (Table 1). That is, ENSO does play a crucial role in the meridional displacement of the AJS. The meridional displacement of the AJS, as the first gravest mode, explains 31% of the total variance and is a significantly separated mode from the others because the second gravest mode only accounts for 10% of the total variance. We also calculated the correlation between ENSO and the next five gravest modes,

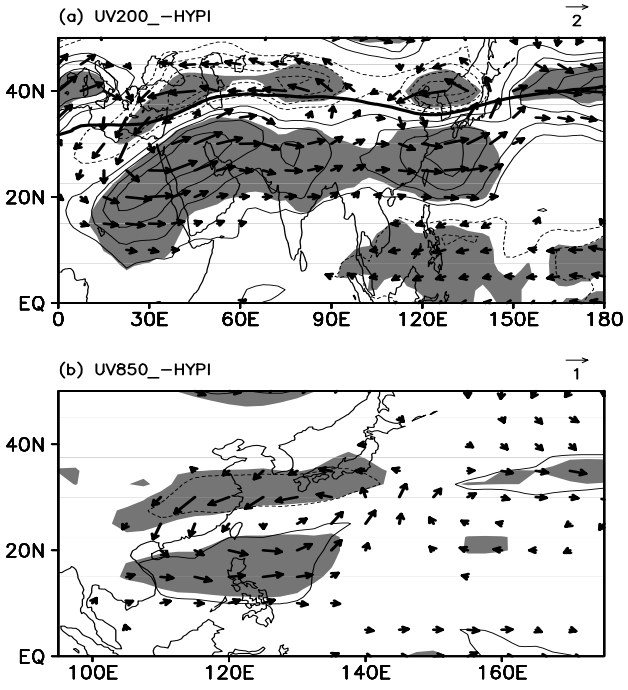

Fig. 8. Same as Fig. 5, but upon the index of minus precipitation averaged in the Huaihe River-Yellow River valleys (31°–36°N, 110°–120°E) (−HYPI) in June.

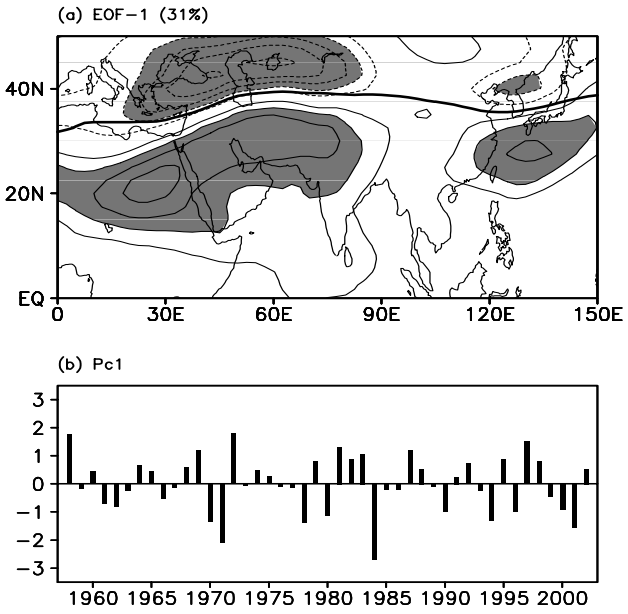

Fig. 9. (a) The first mode of EOF (EOF-1) on the June zonal winds at 200 hPa over 0°–50°N, 0°–150°E and (b) the corresponding principle component (Pc1). The components with the periods larger than 8 years are first subtracted by harmonics analysis before performing the EOF analysis. The thick solid line denotes the axis of the climatological June AJS and the value in the bracket is the ratio of explainable variance by the EOF-1. Zonal winds exceeding 2 m s^{-1} are shaded, the contour interval is 1 m s^{-1}, and the zero contours are omitted.

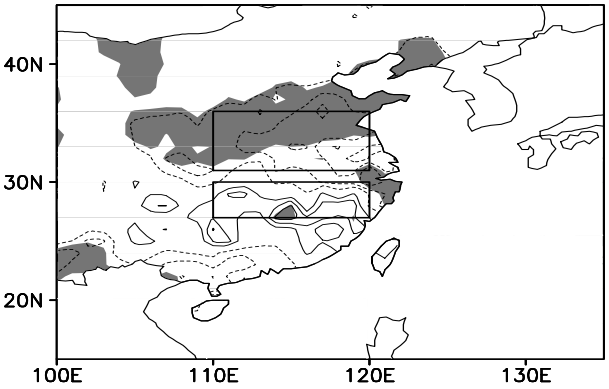

Fig. 10. Same as Fig. 3, but onto the Pc1.

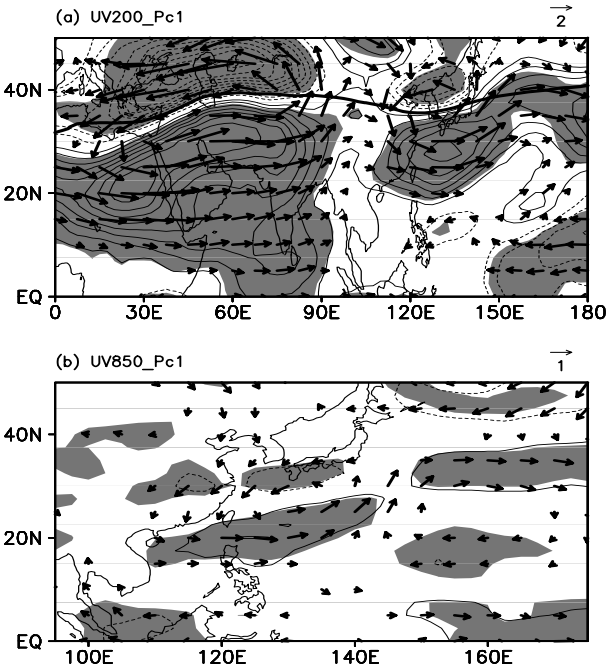

Fig. 11. Same as Fig. 5, but onto the Pc1.

and the coefficients are much smaller and insignificant.

What is the effect of the meridional displacement of the AJS on summer rainfall in eastern China? Figure 10 presents the precipitation anomalies in June related to Pc1. When the AJS shifts southward, the precipitation is remarkably suppressed in the Huaihe River-Yellow River valleys and weakly enhanced in the Yangtze River valley. The correlation coefficients are −0.42 between Pc1 and the HYPI while 0.12 between Pc1 and the YRPI (Table 1).

The effect of the meridional displacement of the AJS on summer rainfall in eastern China is independent of that related to the WNPSMI. The correlation coefficient between Pc1 and the WNPSMI is just 0.12 during the period 1958–2002 (Table 1) and far less significant even at the level of 90%. In the upper troposphere, two strong cyclonic anomalies are located in West Asia and East Asia, respectively, and are related to the southward displacement of the AJS (Fig. 11a), while only a weak cyclonic anomaly in East Asia is associated with the WNPSMI (Fig. 7a). In the lower troposphere, related to the southward displacement of the AJS, a cyclonic anomaly is located over the subtropical WNP and an anticyclonic anomaly appears over the WNP to the east of 140°E (Fig. 11b), similar to the counterpart related to ENSO (Fig. 4b), while clearly separated from that associated with the WNPSMI (Fig. 7b). The cyclonic anomaly, with the northeasterly anomaly across the Huaihe River-Yellow River valleys, weakens the *in-situ* climatological southwesterlies and therefore decreases the northward transportation of moisture into the Huaihe River-Yellow River valleys, resulting in the suppressed precipitation over this region in June.

5. Possible mechanism linking ENSO and the AJS

Recently, Seager et al. (2003) found that in winter and the following spring after an El Niño peak, the zonal-mean (ZM) westerly jet stream in the upper troposphere strengthens in the equatorward flank. They suggested that the variation in the ZM westerly jet stream is related to the increase in the meridional temperature gradient due to the ENSO-related warming in the whole tropical troposphere.

This ENSO-related atmospheric warming in the tropical troposphere persists into the following early summer (Fig. 12a). Related to an El Niño event in the preceding winter, the atmosphere is significantly warmed in the whole tropical region and lower stratosphere in the mid latitudes and weakly cooled in the mid-latitude troposphere. The warming in the tropics increases the tropospheric meridional temperature gradient in the subtropics, and by the thermal balance, leads to the enhancement of westerly flow to the south of the axis of the westerly jet stream (Fig. 13a). The decrease of the meridional temperature gradient by the tropospheric cooling in the mid latitudes, contributes to the ENSO-related easterly anomaly to the north of the axis of the westerly jet stream (Fig. 13a). This opposite-signed extratropical response to ENSO, which is probably related to transient eddies feedback due to the ENSO-related southward displacement of the westerly jet stream (Seager et al., 2003), has also previously been noticed (Yulaeva and Wallace, 1994; Hoerling et al., 2001).

Figure 12b shows the spatial distribution of the ENSO-related averaged temperature anomalies between 300 hPa and 850 hPa. The tropospheric atmos-

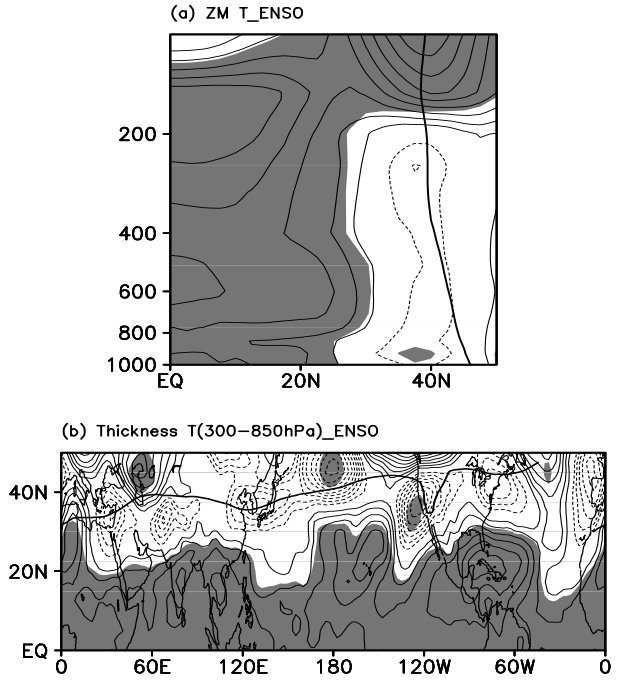

Fig. 12. (a) June zonal-mean (ZM) air temperature (T) and (b) the averaged June temperatures between 850 hPa and 300 hPa regressed onto the preceding DJF Niño-3.4 index. The vertical axis is the pressure level (unit: hPa) in (a). Shading indicates the significance at the confidence level of 95%, contour interval is 0.05 K, and the zero contours are omitted. The thick solid lines denote the axis of the climatological June ZM westerly jet stream in (a) and westerly jet stream at 200 hPa in (b).

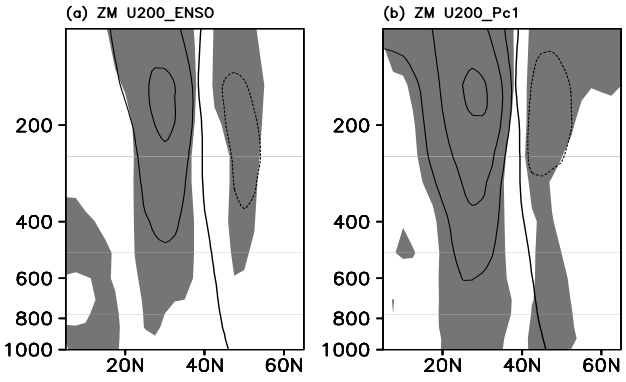

Fig. 13. June ZM zonal winds regressed onto (a) the preceding DJF Niño-3.4 index and (b) the Pc1. The vertical axis is the pressure level (unit: hPa). Shading denotes the significance at the confidence level of 95%, contour interval is 0.5 m s^{-1}, and the zero contours are omitted. The thick solid line represents the axis of the climatological ZM westerly jet stream in June.

phere is significantly warmed in the entire tropical region while cooled in the mid latitudes, consistent with that in Fig. 12a. In the tropics, the centers of warming are located in the Indian Ocean, the central Pacific, the Caribbean Sea, and Africa, leading to the significant enhancement of westerly anomalies to the north (Fig. 14a), due to the increase in the meridional temperature gradient. In the mid latitudes, the weak cooling occurs near the axis of the westerly jet stream in the upper troposphere, and contributes to the easterly anomaly to the north (Fig. 14a). Specially, in the Eastern Hemisphere, the ENSO-related warming in the Indian Ocean and the cooling in the mid-latitudes of Asia, induces the westerly anomaly to move south of the axis of the AJS and the easterly anomaly to move northward, corresponding to the southward displacement of the AJS (Fig. 4a and Fig. 14a).

The southward displacement of the AJS is just one part of ENSO's effect on the zonal flow in the Northern Hemisphere. Figure 13 shows the ZM zonal winds in June related to ENSO and the meridional displacement of the AJS, respectively. Both of them consist of a pair of significant westerly and easterly anomalies in the mid and upper troposphere, which are located south and north of the axis of the subtropical westerly jet stream. The centers of the ENSO-related ZM westerly and easterly anomalies, respectively, are located at about 30°N at 150 hPa and at about 50°N at 200 hPa, coincident to the southward displacement of the AJS.

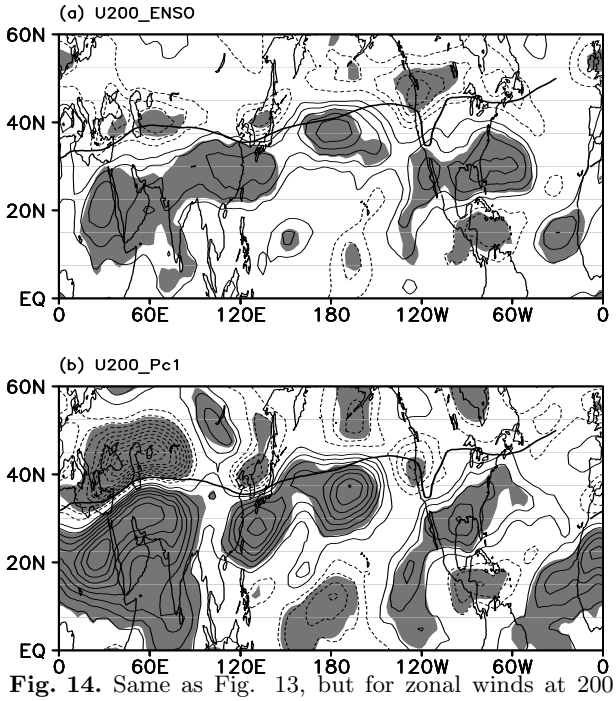

Fig. 14. Same as Fig. 13, but for zonal winds at 200 hPa in June. The thick lines denote the axis of the climatological June westerly jet stream at 200 hPa.

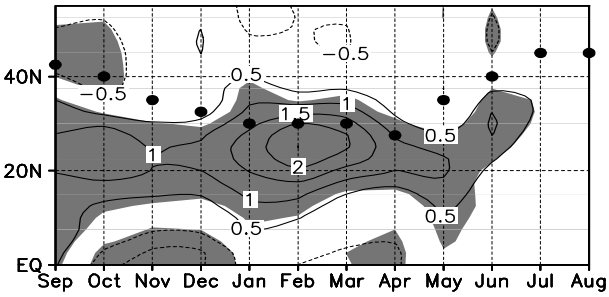

Fig. 15. Monthly ZM zonal winds at 200 hPa from the preceding September to the following August regressed onto the DJF Niño-3.4 index. Shading denotes the significance at the confidence level of 95% and the filled circles depict the locations of the monthly climatological ZM westerly jet stream cores at 200 hPa.

Figure 14 shows the zonal wind anomalies at 200 hPa related to ENSO and the southward displacement of the AJS in the Northern Hemisphere, respectively. Related to El Niño in the preceding winter, the significant westerly anomalies circle around the whole Northern Hemisphere south of the axis of the westerly jet stream, and the weak easterly anomalies appear in West-central Asia, East Asia, and North America north of the axis of the westerly jet stream. The anomalies related to the southward displacement of the AJS are similar to those related to ENSO, and the centers' locations of the zonal wind anomalies are also consistent. It further confirms that the ENSO-related southward displacement of the AJS is just one part of ENSO's effect on the zonal flow in the whole Northern Hemisphere.

These ENSO-related upper-tropospheric zonal wind anomalies only persist through the following early summer, while they disappear in mid summer (Fig. 15). Related to the preceding ENSO, the upper-tropospheric westerly flow strengthens in the equatorward flank of the westerly jet stream from the preceding fall until the following early summer (June), but not in the following mid summer (July–August) in the Northern Hemisphere. This sub-seasonal change in the ENSO-zonal flow in the upper troposphere between early and mid summer, may contribute to the absence of significantly suppressed precipitation in eastern China in July and August as shown in Fig. 1.

6. Conclusions

ENSO's effect on the rainfall in eastern China in the following early summer is investigated by using Chinese station precipitation data and the ERA-40 reanalysis data from 1958 to 2002. In June, after the El Niño peak, the precipitation is significantly enhanced in the Yangtze River valley, while suppressed in the Huaihe River-Yellow River valleys.

ENSO links with the summer rainfall in eastern China possibly through two independent teleconnections: One is related to the western North Pacific (WNP) anticyclonic anomaly in the lower troposphere, and the other is associated with the southward displacement of the Asian jet stream (AJS) in the upper troposphere. The ENSO-related WNP anticyclonic anomaly strengthens the climatological southwesterlies in the Yangtze River valley, and thus transports more moisture into this region leading to the enhanced precipitation in the Yangtze River valley. The ENSO-related southward displacement of the upper-level Asian jet stream (AJS) is associated with a cyclonic anomaly over the subtropical WNP, which weakens the northward transportation of moisture into the Huaihe River-Yellow River valleys, resulting in the suppressed precipitation in the Huaihe River-Yellow River valleys.

The southward displacement of the AJS is contributed by the ENSO-related warming in the whole tropical troposphere. The ENSO-related warming in the tropical troposphere persists into early summer, which increases the meridional temperature gradient and by the thermal wind balance, strengthens the westerly jet stream in the subtropics, which corresponds to the southward displacement of the westerly jet stream in the Northern Hemisphere and the AJS in the mid-latitudes of Asia.

Acknowledgements. The authors thank two anonymous reviewers for the helpful comments. This work was supported by the National Natural Science Foundation of China (Grant Nos. 40725016 and 40221503).

REFERENCES

Chang, C.-P., Y. Zhang, and T. Li, 2000: Interannual and interdecadal variations of the East Asian summer monsoon and tropical Pacific SSTs. Part I: Role of the subtropical ridge. *J. Climate*, **13**, 4310–4325.

Chen, L.-X., M. Dong, and Y.-N. Shao, 1992: The characteristics of interannual variations on the East Asian monsoon. *J. Meteor. Soc. Japan*, **70**, 397–421.

Ha, K.-J., and E. Ha, 2006: Climate change and interannual fluctuations in the long-term record of monthly precipitation for Seoul. *International Journal of Climatology*, **26**, 607–618.

Hoerling, M. P., J. S. Whitaker, A. Kumar, and W. Wang, 2001: The midlatitude warming during 1998–2000. *Geophys. Res. Lett.*, **28**, 755–758.

Huang, R., and Y. Wu, 1989: The influence of ENSO on the summer climate change in China and its mechanism. *Adv. Atmos. Sci.*, **6**, 21–32.

Huang, R., and F. Sun, 1992: Impacts of the tropical western Pacific on the East Asia summer monsoon.

J. Meteor. Soc. Japan, **70**, 243–256.

Kosaka, Y., and H. Nakamura, 2006: Structure and dynamics of the summertime Pacific-Japan (PJ) teleconnection pattern. *Quart. J. Roy. Meteor. Soc.*, **132**, 2009–2030.

Lau, K.-M., K.-M. Kim, and S. Yang, 2000: Dynamical and boundary forcing characteristics of regional components of the Asian summer monsoon. *J. Climate*, **13**, 2461–2482.

Lau, K.-M., and H. Weng, 2001: Coherent mode of global SST and summer rainfall over China: An assessment of the regional impacts of the 1997–98 El Niño. *J. Climate*, **14**, 1294–1308.

Lau, N.-C., and M. J. Nath, and H. Wang, 2004: Simulation by a GFDL GCM of ENSO-related variability of the coupled atmosphere-ocean system in the East Asian monsoon region. *East Asian Monsoon*, C.-P. Chang, Ed., World Scientific Publishing Co., 271–300.

Lim, Y.-K., and K.-Y. Kim, 2007: ENSO impact on the space-time evolution of the regional Asian summer monsoons. *J. Climate*, **20**, 2397–2415.

Lin, Z., and R. Lu, 2005: Interannual meridional displacement of the East Asian upper-tropospheric jet stream in summer. *Adv. Atmos. Sci.*, **22**, 199–211.

Lu, R., 2004: Associations among the components of the East Asian summer monsoon system in the meridional direction. *J. Meteor. Soc. Japan*, **82**, 155–165.

Lu, R., and B. Dong, 2001: Westward extension of North Pacific subtropical high in summer. *J. Meteor. Soc. Japan*, **79**, 1229–1241.

Nitta, T., 1987: Convective activities in the tropical western Pacific and their impact on the Northern Hemisphere summer circulation. *J. Meteor. Soc. Japan*, **65**, 243–256.

Seager, R., N. Harnik, and Y. Kushnir, 2003: Mechanisms of hemispherically symmetric climate variability. *J. Climate*, **16**, 2960–2978.

Tanaka, M., 1997: Interannual and interdecadal variation of the western north Pacific monsoon and the East Asian Baiu rainfall and their relationship to ENSO cycle. *J. Meteor. Soc. Japan*, **75**, 1109–1123.

Uppala, S. M., and Coauthors, 2005: The ERA-40 reanalysis, *Quart. J. Roy. Meteor. Soc.*, **131**, 2961–3012.

Wang, B., R. Wu, and X. Fu, 2000: Pacific-east Asian teleconnection: How does ENSO affect East Asian climate? *J. Climate*, **13**, 1517–1536.

Wang, B., R. Wu, and K.-M. Lau, 2001: Interannual variability of the Asian summer monsoon: Contrasts between the Indian and the western North Pacific-east Asia monsoons. *J. Climate*, **14**, 4073–4090.

Webster, P. J., V. O. Magana, T. N. Palmer, R. A. Thomas, M. Yanai, and T. Yasunari, 1998: Monsoons: Processes, predictability, and the prospects for prediction. *J. Geophys. Res.*, **103**, 14451–14510.

Wu, R., Z.-Z. Hu, and B. P. Kirtman, 2003: Evolution of ENSO-related rainfall anomalies in East Asia. *J. Climate*, **16**, 3742–3758.

Yulaeva, E., and J. M. Wallace, 1994: The signature of ENSO in global temperature and precipitation fields derived from the microwave sounding unit. *J. Climate*, **7**, 1719–1736.

Zhang, R., A. Sumi, and M. Kimoto, 1999: A diagnostic study of the impact of El Niño on the precipitation in China. *Adv. Atmos. Sci.*, **16**, 229–241.